PAHST

Polycyclic Aromatic Hydrocarbons Space Telescope
Mission Proposal

Team Blue:

Raphael Böckle, Adam Byrne, Jeremy Chastenet, Isabella Cortzen, Sergio Díaz Suárez,
Esfandiar Farahvashi, Alessandro Fasano, Martin Glatzle, Adina Godeanu,
Dorota Jozwicki, Soheb Mandhai, Jelle Mes, Embla Morast, Laura Selliez, Inna Uwarowa

Team Blue Tutors:

Jaan Praks (engineering), Vera Könyves (science)

Executive Summary This paper presents the *Polycyclic Aromatic Hydrocarbons Space Telescope* (*PAHST*) mission. *PAHST* will probe star formation in the Early Universe by detecting PAH features and emission lines redshifted to $30 - 200$ μm at $4.5 < z < 7$. Secondly, we propose to study the high density filaments in the Interstellar Medium (ISM) of our Galaxy to characterise their inner structures. We are also interested in studying not only the nature of cool brown dwarfs but the presence of dusty discs there. The Lagrange point 2 is selected as the suitable orbit for the observations and the mission is prepared for launch with an Ariane 6 rocket. The spacecraft features 8 m mirror IR telescope equipped with a high sensitivity spectrometer and photometer.

Mission parameters

Mission type: IR Space Telescope
Target Orbit: L2
Mirror size: 8 m
Detector A: Photometer
Detector B: Spectrometer
Wavelength range: $30 - 200$ μm
Mission lifetime: 5 y
Spacecraft dry mass: 5699 kg
Mission class: L
Mission cost: 2.43 G€

---

1 Scientific Objectives

The primary aim is to probe star formation in distant galaxies using near-infrared (NIR) tracers. At these redshifts, the observational range falls in the far-infrared (FIR) domain. In the following report, these scientific cases are described in detail.

Primary Science Driver: Previous observations have revealed that the star formation activity peaked approximately 10 billion years ago, where galaxies formed the bulk of their stellar mass around $z \sim 2$ (Carilli & Walter 2013; Madau & Dickinson 2014). The cause of this evolution is unknown, although a possible explanation around $z \sim 2$ may be due to higher gas infall from the intergalactic medium onto galaxies, which leads to larger amounts of gas and higher star formation rates. At $z < 2$ previous studies reveal the importance of infrared (IR) coverage to probe the obscured star formation by interstellar dust in galaxies (Figure 1; Madau & Dickinson 2014). At high-z the ultraviolet (UV) measurements are corrected for dust absorption. Since the extrapolations are based on local galaxy models, IR observations of the obscured star formation at high-z becomes evident. Gaining insight to the complete star formation within galaxies in the early Universe will enhance our understanding of the physical processes that shaped the evolution of star formation across cosmic time.

The proposed space telescope mission will detect the polycyclic aromatic hydrocarbon (PAHs; carbonaceous planar molecules) emission to probe star formation within galaxies in the early Universe. Their emission features (namely 6.2 μm, 7.7 μm, 8.6 μm and 11.3 μm) dominate the mid-IR (MIR) spectrum of a star-forming galaxy, arising from photodissociation regions (PDRs). This emission is produced when UV photons from young stars heat up the molecules, and it can therefore be used to trace the obscured star formation within galaxies. Previous studies based on local and intermediate-redshift galaxies have established a linear correlation between the star formation rate (SFR) and the PAH emission. For example, Peeters et al. (2004) have shown that the observed PAH intensity can be used as
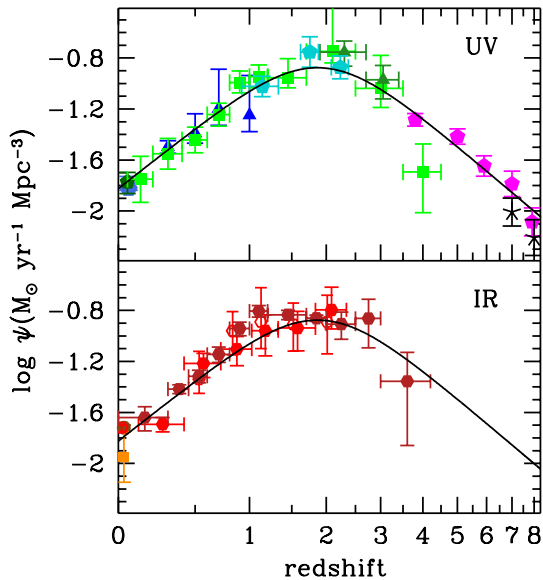
Figure 1: A compilation of the star formation rate density, ψ, deduced from galaxy surveys noted in the literature up to $z = 8$ (Madau & Dickinson 2014). Upper and lower graphs are based on observations in UV and IR regions, respectively.
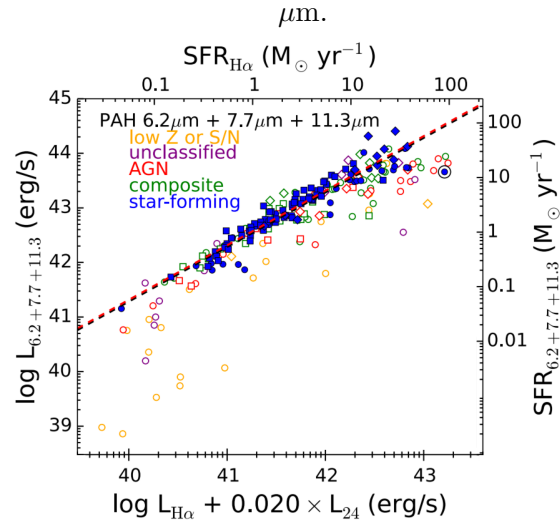

Figure 2: Correlation between PAH and Hα luminosities for 105 star-forming galaxies at $0 < z < 0.4$. Figure modified from Shipley et al. (2016).

a proxy of SFR in the Galaxy (see also Figure 2; Shipley et al. 2016). The variations in strength of the PAH features combined with MIR emission lines, including H$_2$, [Ne II] and [Ne V], reveal physical properties of the dust distribution including metallicity and ionization state (e.g. Petric et al. 2011, and references therein). The H$_2$ emission lines H$_2$S(0) and H$_2$S(1) at 17.1 μm and 28.8 μm will allow us to probe the warm molecular gas in our targets. We expect a significant amount of such gas where star formation occurs, as it is a necessary fuel for star formation. However, H$_2$ detections are pendant on its ionization state, which may arise from three sources: UV photons, shocks, and AGN irradiation. The contribution of the UV photons to the H$_2$ excitation will be determined through the PAH features detections. The AGN contribution can be measured by the Neon lines [Ne II] 15.6 μm and [Ne V] 14.3 μm, which unveil the presence of such an object. We will provide measurements of these lines to disentangle with more accuracy the influence of each star formation tracers. Combined with ground-based facilities including ALMA, we will be able to observe the cold molecular gas using excited CO lines and [C II]. The ratio of the total available molecular gas reservoir to the SFR indicates how efficiently

gas is being turned into stars. It can thus be used to distinguish the star formation activity in normal and merger-induced starburst galaxies. Linking the PAH features with both cold and warm molecular gas in a sample of thousands of distant galaxies will provide crucial information of the ongoing star formation and the dust properties within these distant sources. The redshifted wavelengths previously mentioned lead us to a spectral coverage from 30 to 200 μm.

The main driver for resolution when aiming to observe faint FIR sources is confusion. To obtain a complete picture of star formation, it is necessary to observe sources down to the characteristic magnitude M^* of the luminosity function. Using M^* at $3 < z < 11$ from Bouwens et al. (2015, Table 6), we computed the IR luminosity of such an object according to $L_{IR} [L_\odot] \propto 10^{10} \times$ SFR $[M_\odot$ yr$^{-1}]$ (Kennicutt 1998) where SFR is the star formation rate given by Equation 5 in Bouwens et al. (2015). We then used spectral energy distribution (SED) templates for main-sequence galaxies up to $z \approx 2$ from Elbaz et al. (2011) to estimate the expected spectral flux density in PAH features as a function of redshift. Berta et al. (2011) provide 70 μm number counts which allow us to estimate the required angular resolution. Assuming 10 beams per source are required to resolve a galaxy against the background, we estimate the required angular resolution as a function of redshift (Figure 3). We con-
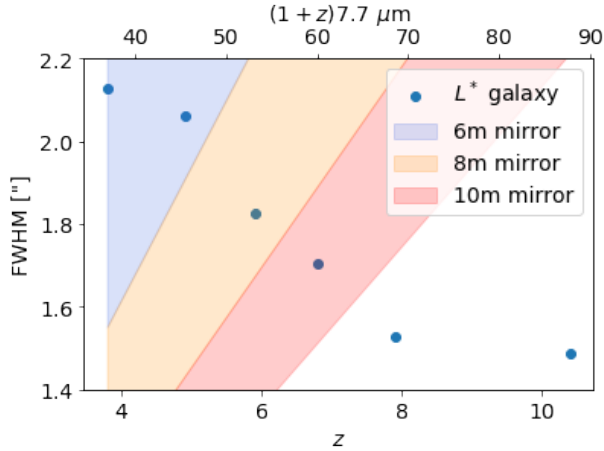
Team Blue

Figure 3: Angular resolution as a function of redshift. The coloured regions correspond to diffraction limits of various mirror sizes.
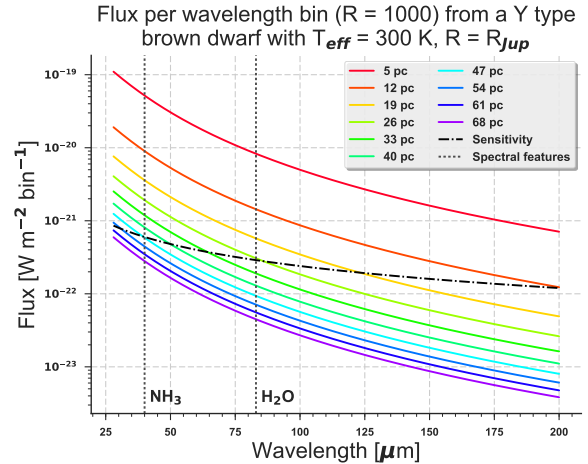

Figure 4: Expected flux from a Jupiter-size brown dwarf with $T_{\mathrm{eff}} = 300$ K at various distances from the Sun, compared to the sensitivity of our detectors (dash-dotted line).

clude that a mirror diameter of 8 m is required to constrain obscured SFR at $z \sim 6$.

Secondary Science Case: Recently, *Herschel Space Observatory* observations confirmed the ubiquity of filaments in Galactic molecular clouds and suggested an intimate connection between these cold structures of the ISM and the formation of stars. Up to a distance of ~ 1.7 kpc, the filaments are resolved with *Herschel* and with ground-based observations in the sub-mm range (see André et al. 2016). The characteristic inner width of the filaments is found to be $W_{\mathrm{fil}} \sim 0.1$ pc (Arzoumanian et al. 2011), and typically a large fraction of dense star-forming cores are sitting inside them (e.g., Könyves et al. 2015).

At larger distances, few pc-wide elongated structures with high column density ($>$ 10^{23} cm^{-2}) are called "ridges" (see Hill et al. 2011), and are thought to provide necessary conditions for clustered high-mass star formation. These gravitational wells could have been formed by dynamical scenarios such as converging flows, which are channelling dust and gas and show signs of global infall. High-mass stars (OB-type, $M_* > 8$ $M_\odot$) play a major role in the energy budget and enrichment of galaxies, but their formation remains poorly understood (unlike that of solar-type stars). The above dynamical ridge formation process is proposed to explain the formation of OB stars (Heitsch et al. 2006).

In order to see the details of high-mass star formation, and resolve whether these ridges are merging from individual filaments of ~ 0.1 pc, we are aiming to use the photometer (channel 3 at ~ 150 μm) onboard *PAHST*. We will map ridges up to our ability to resolve their inner widths ($d \sim 2 - 4$ kpc). We select the ridge sample from the HOBYS *Herschel* programme (Motte et al. 2010); e.g., ridge G035.39–00.33 in the W48 star-forming molecular complex at ~ 3 kpc (Nguyen Luong et al. 2011).

Tertiary Science Case: Brown dwarfs are substellar objects that are unable to fuse hydrogen in their core due to their low mass ($M < 0.08$ $M_\odot$). However, they are able to fuse elements such as lithium, and under these conditions, are still able to form dusty discs. Despite NIR imaging of the multiple ring systems surrounding brown dwarfs, observations at longer wavelengths ($\lambda > 24$ μm) are missing to probe their cooler outer disks (Zakhozhay et al. 2016). The high sensitivity of *PAHST* in the MIR/FIR is well-suited to study such objects. We will be able to observe the colest brown dwarfs of class Y, which were recently discovered (Cushing et al. 2011). We can use the spectral lines of NH$_3$ at 40 and 42 μm to distinguish between T and Y class dwarfs (Delorme et al. 2008). Figure 4 shows the expected flux from a Jupiter-size brown dwarf with $T_{\mathrm{eff}} = 300$ K at different distances from the Sun. The *WISE* mission detected 300 K dwarfs up to 6 pc from the Sun. The *PAHST* spectrometer will be able to detect these up to $d \sim 26$ pc and resolve the H$_2$O and NH$_3$ features. We will be

Team Blue

Table 1: Overview of key science requirements for the mission. *: At a wavelength of 50 μm.

Parameters	Values
Angular Resolution["]*	1.6
Number Count[sr^{-1}]	10^9
Sensitivity[μJy]	8
Spectral Range [μm]	30 - 200
Spectral Resolution (R)	1000
Mission time	5 years

able to probe $\sim$ 77 times more Y class brown dwarfs than *WISE*.

The science requirements are derived from mission objectives and are summarised in Table 1.

2 Mission Design

2.1 Requirements and Design Drivers

The mission requirements are derived directly from the science requirements (Table 1). Additionally, it is required that ESA launchers are used and that the spacecraft is disposed of after the mission.

2.2 Orbit

For a space telescope mission the best orbit near Earth is Lagrange Point L2, as proven by earlier successful missions, such as *Herschel*, *Planck* and *Gaia*. The *James Webb Space Telescope* will be placed at L2 as well. The orbit provides stable conditions essential for the demanding thermal design, and the *PAHST* is designed for placement at L2. The spacecraft requires very low temperatures in order to achieve the required signal-to-noise (S/N) ratio. Position at L2 also improves the reliability and the performance of the satellite. A large amplitude orbit, either Halo or Lissajous, is selected to avoid eclipse by Earth. The orbit will eventually provide feasible end-of-life disposal option to solar orbit.

2.3 Launcher

Out of the currently available launchers only Ariane 5 has the capability to insert *PAHST* into an L2 halo orbit. However, since Ariane 5 is to be phased out before the launch of *PAHST*, mission planning was performed assuming an Ariane 6 launch. The Ariane 6 launcher provides better capacities, a larger fairing, and its highly elliptical orbit (HEO) performance is 7 000 kg (Lagier 2016). The usable volume beneath the payload fairing in a single launch is 11.185 m, up to the fairing conical shape transition and the diameter is 4.570 m. In order to fit to the launcher envelope, the largest spacecraft structures including the telescope mirror sunshade shall be folded for launch (Perez 2001). The total launch cost is estimated to be 175 M€.

2.4 Observation Strategy

To perform observations at L2 orbit, the direction of the sunshield sets severe restrictions on observation strategy as the telescope mirror shall be always in shadow. Target definition will follow two strategies. First, we aim at mapping the GOODS-N and GOODS-S of the *HST* Deep Fields with our photometer in the three available photometric bands centred at $\sim$ 50, $\sim$ 90, and at $\sim$ 150 μm. *HST* observed the distant Universe in the Visible/NIR domain down to redshift $z \sim 10$, providing a large amount of measurements. The *Spitzer Space Telescope* also covered some of the *HST* Deep Fields, extending the already available SED. Using the same sky coverage as the available data will allow us to cross-match our sample with the existing UV/NIR-detected galaxies. Performing statistical analysis of the detected IR population of galaxies in the early Universe will reveal the dominant galaxy population at these redshifts. A comparison with existing observations in the UV regions will clarify the possible selection bias based on the UV observations.

Our second goal is to perform follow-up spectroscopic observations of the galaxies found in the GOODS fields. Targets will be selected based on the results from the IR mapping. The science requirements for these observations are listed in Table 1.

2.5 Ground Segment

To establish a ground link with L2 orbit, two ESA ground stations have been selected. The primary ground station is Cebreros in Spain, and the secondary station is Malargüe in Argentina. The required link time should not exceed 6 hours,

so that one shift can handle the communication at ESOC. Two frequency bands are selected according to mission data rates and available ground stations. The Ka-Band will be used as the downlink from the satellite and X-Band is dedicated for uplink. X-Band and Ka-Band were chosen, because both bands were already used in other missions and are therefore approved. Additionally, both bands are available at the two ground stations.

2.6 Disposal

According to the Space Debris regulations, at the end of it's life a spacecraft will be removed from the operational L2 large amplitude orbit to a heliocentric orbit. The ΔV calculations for this manoeuvre are presented in Section 3.4. A 50% margin for this manoeuvre was taken into account; sufficient amount of fuel will be reserved.

3 Space Segment Design

Driven by science requirements, a spacecraft was designed to carry *PAHST*: an IR telescope with a diameter of 8 m, a large sunshield and a V-groove type of passive cooling of the telescope. The concept is depicted in Figure 5. In order to fit the required 8 m diameter mirror in the fairing, a mirror folding concept was developed. The satellite is depicted in the fairing in Figure 6. The sunshield and V-groove cooling system area need to fit into the available space in the launcher. The mirror folding technique, similar to *JWST*, was selected where the side sections of the mirror are hinged to the sides of the spacecraft. The folding sunshield, similar to *GAIA* spacecraft, was selected for sunshield technology.

The overview of the mass and power budget is given in Table 3. Margins on subsystem level are applied according to the TRL levels. Additionally, an overall 20% system margin was considered for the dry mass of the spacecraft. The masses of the subsystems are assumed based on previous space missions.

3.1 Folding Mirror Telescope Design

The optical requirements for this telescope call for high angular resolution, small diffraction limited field of view (DLFOV) and carries the obvi-
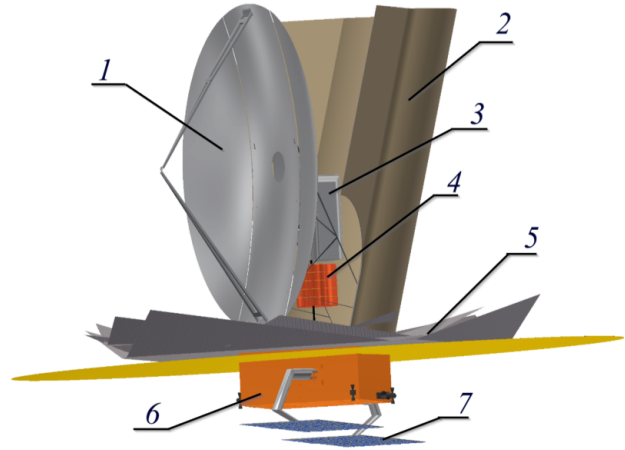

Figure 5: *PAHST* spacecraft. Main mirror (1), Al thermal shield (2), detectors (3), cryogenic systems (4), V-groove passive cooler (5), service module SVR (6), solar panels (7).

ous constraint that it must fit in the volume of an Ariane 6 fairing. Off-axis telescope designs are more compact. However, they suffer from a number of drawbacks that make them unsuitable for our purposes, the most important of which is the limited system focal length due to the compact design. On-axis configurations offer larger, symmetric mirrors but are longer in the vertical axis. Of these on-axis designs, the Cassegrain is a classic and often used choice for space telescopes such as *Herschel*, *Spitzer* and the *Hubble Space Telescope*. The design used for this mission is a hyperbolic primary mirror coupled to a hyperbolic secondary. This variant is known as a Ritchey-Chrétien and has the advantage that coma and spherical aberration are eliminated. Henceforth the primary mirror will be referred to as M1 and the secondary as M2. The parameters of the telescope are listed in Table 3. The surface of M1 is flat, which makes better use of the launcher volume. The focus of the system was chosen to be 1 m below M1. This helps to isolate the instrument from the primary mirror and to maintain the 4 K mirror temperature. The mirrors themselves will be constructed from SiC with a few micron thick coating of aluminium. This process will be the same as that used to construct *Herschel's* mirrors (Garcia-Lario et al. 2014). *SPICA* also plans to use the same materials due to their reduced mass (Collaboration et al. 2009).

The process of unfurling the telescope will be staged. The solar array will need to be deployed

Table 2: Mass and Power budget overview on subsystem level. Values given with margins on subsystem level w.r.t. the TRL levels.

	Subsystems	TRL level	Mass (kg)	Peak Power (W)
Service Module	Solar Arrays	8	88.00	N/A
	Power Control	8	35.20	38.50
	Harness	8	99.60	N/A
	AOCS	8	69.30	62.70
	Structure	4	420.00	N/A
	Thermal Control	6	330.00	176.00
	Data Handling	8	31.50	110.00
	Communication	7	23.10	27.50
	Sunshield	4	720.00	N/A
Sum SM			1816.70	414.70
Payload	Optics and Structure	4	2160.00	N/A
	Detectors & Data Processing	6	50.60	22.00
	TCS	6	252.00	1281.50
	Structure	4	360.00	N/A
	Harness	8	110.00	N/A
Sum Payload			2932.60	1303.50
S/C Sum			4749.30	1718.20
Sys. Margin (%)			20.00	20.00
Total Sum			5699.16	2061.84
Propellant			410.24	
Total Wet Mass			6110.00	

Table 3: Optical parameters of *PAHST*.

Telescope Parameters	
M1 Diameter	8 m
M1 Focal Length	6.1 m
M1 Radius of Curvature	12.2 m
M2 Diameter	0.5 m
M2 Focal Length	7 m
M2 Radius of Curvature	0.2 m
M1 - M2 Separation	6 m

soon after launch. Once it has arrived at L2, the telescope will deploy it's sunshield and begin the process of cooling. Actuators located on the back plane of the telescope will move the two folded mirror segments into place. A system similar to that on *JWST* will ensure that the mirror geometry is properly realigned by attempting to match the segment radius of curvature to that of the primary mirror.

The instrument optical chain begins at the system focus of the telescope. An offset parabolic mirror is used to collimate the beam from the telescope, which will be required for spectrometry. The focal plane field stop contains two apertures: one for the photometry channels and one for the spectroscopy channels. The choice of instrument mode is controlled by positioning the source to be located at the centre of either aperture. This is a common operation in multifunctional instruments and has been used on PACS (*Herschel*) (Garcia-Lario et al. 2014) and IRS (*Spitzer*) (Garcia-Lario et al. 2014).

For the photometric optical train, dichroic filters are used for channel selection. It is imperative that as few photons as possible are absorbed by the optics to maintain the sensitivity required. Dichroic filters reflect rather than absorb radiation whose wavelength has not been selected for. This property makes them very common in channel selection in instruments. Radiation that is reflected by the dichroic will be rerouted to a folding mirror to redirect it to the other channels. This propagation continues until the end of the three channels. Past each dichroic will be a filter wheel containing a high and low wavelength filter as well as a free space aperture. After this
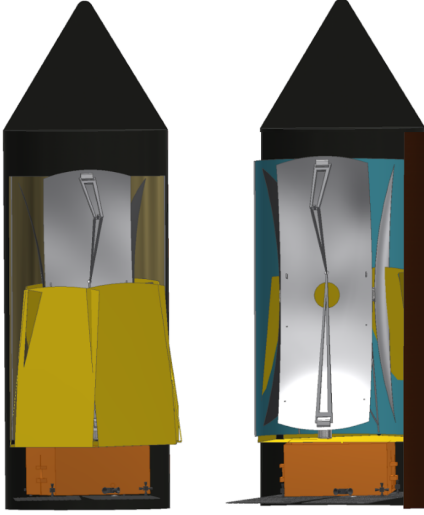
Figure 6: The *PAHST* spacecraft in stowed configuration in the Ariane 6 fairing.

refocusing optics (parabolic mirror) will be used to focus the radiation onto the detector.

The spectrometer optical chain is quite similar to the photometric one. The radiation will fall first onto an image slicing mirror similar to that used in PACS. This will arrange the image into a series of one dimensional cuts. These cuts will be recombined after reflection from the grating. Channel selection occurs identically to the photometry channel, using dichroic filters to separate the three channels. As with photometry, filter wheels shall be present in each channel. The radiation will then be focused onto the relevant detectors.

3.2   Detectors

PAHST is an 8 m diameter IR telescope with a cryogenically cooled mirror at 4 K. Cooling the optics reduces the background radiation caused by the ambient temperature of the telescope that limits the sensitivity. The loading is then dominated by astrophysical background sources and the intrinsic photon noise limitation due to Bose-Einstein distribution of the photons. In the range of $30 - 200 \mu$m the background is dominated by emission from the Zodiacal light, which gives an intrinsic photon noise equivalent power $\text{NEP}_{photon} \sim 10^{-18} \frac{W}{\sqrt{Hz}}$. We require detectors with electrical NEP at least 3 times lower than the photon noise limit $\left(< 3 \cdot 10^{-19} \frac{W}{\sqrt{Hz}} \right)$. The detecting instrumentation choice is based on two

Table 4: Channel specifications.

	CH 1	CH 2	CH 3
Central λ [μm]	47	87	155
Range λ [μm]	30-64	64-100	110-200
Angular Resol. ["]	1.48	2.74	4.89
FoV [']	0.50	0.46	0.49
Pixels [photom.]	40x40	20x20	10x10
Pixels [spectro.]	430	300	1600

issues: maximise the sensitivity and sampling each beam with 4 pixels.

The Transition Edge Sensor (TES) is the selected detector technology for this mission. SRON is developing low thermal conductance TES bolometers with NEP achieved of $\sim 3 \cdot 10^{-19} \frac{W}{\sqrt{Hz}}$ and it is expected to reach the value of $\sim 5 \cdot 10^{-20} \frac{W}{\sqrt{Hz}}$ for the future. The absorption section is coupled with the radiation through a conical horn in order to optimise the absorption. The size of the pixel is of 850 μm (SAFARI's mid-wavelength band pixels). The multiplexing capability of the TES technology allows to use one SQUID readout system for every 160 pixels (Jackson et al. 2011). The angular resolution, as a function of the band observed λ, is fixed by the diameter of the telescope D (8 m) by the equation: $\theta_{res} = 1.22 \cdot \frac{\lambda}{D}$.

The choice for the number of pixel is thus fixed by the Field of View required, the *PAHST* mission will sample the single beam with 4 pixels: $N_{pix} = 4 \cdot \frac{FoV}{\theta^2}$. In Table 4 there are listed all the specifications for every channel.

3.3   Thermal Design

The cryogenic system is designed to provide required 4 K temperature for the main mirror and 50 mK for the focal plane detectors.
The 4 K temperature of the mirror minimises optical load contribution to the system and the 50 mK temperature at the final stage allows for the use low noise detectors, which will maximise the sensitivity of the system. The architecture of the cooling system is depicted in Figure 7.

The system is composed of common passive cooling system, composed by sunshield, three V-grooves and a cooled aluminium shield in a configuration where the passive system is followed by an active system. The design provides a bi-
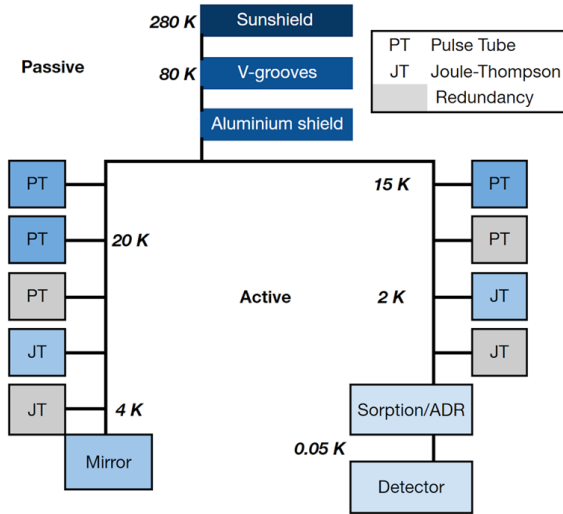
Team Blue

Figure 7: Scheme of the cryogenic chain.

furcated system for both the mirror and the detector. The mirror reaches a temperature of 4 K with a two stage double Pulse-Tube and Joule-Thompson cooler. For the focal plane, two stage Pulse-Tube and Joule-Thompson coolers in conjunction reach 2 K. Finally, the detectors are cooled to 50 mK with a Hybrid Sorption/ADR. Both the active systems are part of a complete redundancy. This requirement mitigates the risk of malfunctioning on the part of the mechanics of the cooling system. The cooling cycle of the Hybrid Sorption/ADR is 48 hours with a duty cycle of 75% (Duband 2016) representing an upper limit to the integration time of the telescope. This value is perfectly compatible with the 20 hour integration time required by this mission.

3.4 Attitude and Orbital Control System

PAHST has an active 3 axis stabilisation system, with stringent pointing requirements imposed by the science instruments (Larson & Wertz 1992). In order to perform scanning, the spacecraft will be rotating around the z axis. A 1" pointing accuracy with 0.1" pointing knowledge is required to fulfil the instrument requirements. The spacecraft L2 operation orbit puts the constraints on the type of sensors and actuators that can be used for attitude determination and control. Attitude and Orbital Control System (AOCS) component choices were made considering orbital manoeuvres, spacecraft mass, moments of iner-

Table 5: ΔV values for orbit initialisation as well as attitude and station keeping.

Manoeuvre	Margin(%)	ΔV (m/s)
Launcher Dispersion	50	67.5
Station Keeping	50	4.5
RW Desaturation	100	10
EOL Disposal	50	15

tia, pointing accuracy, re-pointing requirements, mission lifetime, spacecraft dimensions, components flight heritage, mass and power requirements. For the lower accuracy operations, the set of sun sensors and gyroscopes had been proposed. The required high determination accuracy will be covered by the star trackers. As for orbital manoeuvres and re-pointing actuators, a set of 12 monopropellant hydrazine 20 N thrusters with $I_{sp} = 230$ s will be used. For the final pointing corrections a set of 4 reaction wheels has been proposed.

For calculating the required propellant mass for the thrusters, four types of maneuvers were considered for the mission duration. The types of maneuvers as well as the corresponding ΔVs are presented in Table 5. The ΔVs are given by (Alessi et al. 2014) and E. Montagnon (priv. comm.) for a mission to an L2-Orbit. Hereby, the Launcher Dispersions also include the orbit injection errors. For the ΔV budget, a dry mass of 5699.16 kg was considered (see Table 3). For calculating the required propellant mass, two scenarios with 5 year and 10 year mission duration were analysed. The analysis showed that an increase of 18.31% of the required propellant mass will result in a 100% increase of the mission duration. This is due to the fact that an increase in mission duration will only need additional propellant mass for station keeping, requiring the lowest amount of ΔV compared to the other manoeuvres. Therefore, a propellant mass of 410.24 kg is considered for the spacecraft for a mission duration of 10 years, and the resulting wet mass of 6110 kg will still be suitable for a launch with Ariane 5.

Team Blue

3.5 Communication System

The amount of data which is being produced by the detectors during "Science Mode" was estimated to be 4 MB/s, similar to other space telescopes like *Herschel* (Garcia-Lario et al. 2014) and *Planck*. For *PAHST* the maximum observation time is 38 hrs, corresponding to a maximum of 600 GB of data.

Furthermore, the X-Band and Ka-Band have been chosen for communication. The X-Band (operating at 8.4 GHz) is used for the uplink and the Ka-Band (operating at 32 GHz) as the downlink for the measurement data. In Section 2.5 the advantages of these two bands have been described.

The measurement data is stored in the memory unit and will be sent to the ground segment as soon as possible. The time-frame is 3 h/day to send the data to the ground segment. More details can be found in Section 2.5.

Table 6 gives an overview of the link budget and the used transmitter. The maximum data rate, being the measurement (Ka-Band) and control/overhead (X-Band) over the defined medium, allows enough margin to transmit data.

For the internal communication of the satellite *SpaceWire* will be used, because this bus system is already established; e.g. *Gaia* used *SpaceWire* as well.

3.6 Power System

The power system is set up by solar panels and a battery. The electrical power of the battery is only used during launch and positioning of the

Table 6: Communication link parameters.

Parameter	Values
Transmitter power	15 W
Transmitter dish size	0.2 m
Downlink	
X-Band operating frequency	8.4 GHz
X-Band maximum data rate	66 GB/h
X-Band final EB/EN	31.7 dB
Uplink	
Ka-Band operating frequency	32 GHz
Ka-Band maximum data rate	956 GB/h
Ka-Band final EB/EN	43.3 dB

Table 7: Overview of required power generation and solar panel area. A system margin of 20% was considered for power demand and solar panel area.

Parameters	Values
Solar Cell Type	Triple-Junction InGaP/InGaAs/Ge
Efficiency	29.5%
Solar Illum. Power	1340 W/^{2}
Mission Duration	5 years
Power at BOL	243.5 W/m^2
Power at EOL	178.7 W/m^2
Power Demand	2061.84 W
Req. S/P Area	13.84 m^2

spacecraft at the very beginning of the mission. For the calculation the mission modes were analysed and the battery capacity was calculated using a energy density of 200 Wh/kg.

The required power was determined by analysing various mission modes such as 'Repositioning' and the 'Science' mode. The analysis showed that in the science mode the subsystems demand the most power, since the scientific instrument have high power requirements. The power consumption during science mode is summarised in Table 3. Using these numbers, a solar panel area of 13.84 m^2 was calculated w.r.t. the power demands of the science mode (see Table 7).

4 Programmatics

4.1 Schedule and Cost

The *PAHST* mission is scheduled for 17 years from now, 12 years of which will be the development phase including 5 years of production. The telescope has an operational lifetime of 5 years before disposal.

The total cost of the mission is estimated to 2.43 G€, of which 2.13 G€ is ESA budget and 300 M€ is contribution from member states. The estimation is based on the total cost from previous missions, i.e. *Herschel* (Garcia-Lario et al. 2014), and *JWST*. The size and design of the telescope introduce an uncertainty in the cost estimation, as the production of the *JWST* has shown this can be unpredictable. The first estimation for

the telescope production is 400 M€.

In Table 3 the most critical components are listed with the corresponding TRL levels. The critical technology development should get special attention.

4.2   Risks

The most severe risks of the *PAHST* mission are related to technology development, orbital injection failure and malfunction of various subsystems (Sunshade, ADCS, OBC, software, communication), which could cause a loss of the mission. The likelihood of such a scenario is low, but significant attention shall be given to testing of critical components. Risks with higher likelihood are mainly related to delays in schedule and corresponding costs, which can be considered as less severe as it does not endanger the mission. Minor delays regarding launching can be accepted, as the mission is not dependent of launch window.

5   Final Remarks

While ground-based telescopes offer a great advantage in the sub-mm wavelength range, in the FIR domain we are restricted to carry out space missions. They are generally high risk and expensive projects, although their science gain is of extreme importance. The presented facts and figures confirm that the above proposed *PAHST* mission is best suited in collecting additional higher quality data for clarifying long-standing questions of star- and planet formation; in our Galaxy, as well as in the early Universe.

References

Alessi E. M., Colombo C., Landgraf M., 2014, in 24th International Symposium on Space Flight Dynamics. pp 5–9

André P., et al., 2016, A&A, 592, A54

Arzoumanian D., et al., 2011, A&A, 529, L6

Bandecchi A. L. M., 2006, ESA

Berta S., et al., 2011, A&A, 532, A49

Bouwens R. J., et al., 2015, ApJ, 803, 34

Carilli C. L., Walter F., 2013, ARA&A, 51, 105

Collaboration S. S. T., et al., 2009, ESA/SRE, 6, 2009

Cushing M. C., et al., 2011, The Astrophysical Journal, 743, 50

Delorme P., et al., 2008, A&A, 482, 961

Duband L., 2016

Elbaz D., et al., 2011, A&A, 533, A119

Garcia-Lario P., Merin B., Sanchez-Portal M., Kidger M., 2014, Herschel Observers' Manual Chapter 2, Website, http://herschel.esac.esa.int/Docs/ Herschel/html/ch02.html#sec2:SVM

Heitsch F., Slyz A. D., Devriendt J. E. G., Hartmann L. W., Burkert A., 2006, ApJ, 648, 1052

Hill T., et al., 2011, A&A, 533, A94

Jackson B., et al., 2011, The SPICA-SAFARI detector system: TES detector arrays with frequency division multiplexed SQUID readout. International Symposium on Space Terahertz Technology, pp 46–49

Kennicutt Jr. R. C., 1998, ApJ, 498, 541

Könyves V., et al., 2015, A&A, 584, A91

Lagier R., 2016, Ariane 6 User's Manual. Arianespace, issue 0 revision 0 edn

Larson W. J., Wertz J. R., 1992, Technical report, Space mission analysis and design. Microcosm, Inc., Torrance, CA (US)

Madau P., Dickinson M., 2014, ARA&A, 52, 415

Motte F., et al., 2010, A&A, 518, L77

Nguyen Luong Q., et al., 2011, A&A, 535, A76

Peeters E., Spoon H. W. W., Tielens A. G. G. M., 2004, ApJ, 613, 986

Perez E., 2001, Ariane 5 User's Manual. Arianespace, issue 5 revision 1 edn

Petric A. O., et al., 2011, ApJ, 730, 28

Shipley H. V., Papovich C., Rieke G. H., Brown M. J. I., Moustakas J., 2016, ApJ, 818, 60

Zakhozhay O., Rosa Zapatero Osorio M., Sánchez Béjar V. J., Boehler Y., 2016, 41